RADIOMETRIC NORMALIZATION OF LANDSAT ETM+ DATA FOR MULTITEMPORAL ANALYSIS

M. Caprioli, B. Figorito, E. Tarantino*

DVT- Polytechnic University of Bari -Italy
E-mail*: m.caprioli@poliba.it; benedetto1980@libero.it; e.tarantino@poliba.it*

KEYWORDS: Multitemporal analysis, Radiometric normalization, Empirical Line Calibration, MAD transformation.

ABSTRACT

The advantages of Remote Sensing for the knowledge of environmental dynamics are widely ascertained by scientific community. Spatial synchronization and temporal resolution of large areas have meaningfully improved quantity and quality of satellite imagery which have assumed an important role in the field of environmental monitoring. Nevertheless, preliminary processing problems of multitemporal satellite data, as basic information in the analysis of land cover transformations, persist because of errors due to noise, to environmental conditions and to geometric and radiometric distortions introduced during the acquisition and the transmission phases.

The methods of radiometric normalization for multitemporal analysis of satellite imagery can be absolute and relative. The absolute methods are not always feasible because they need to measure the optical properties of the atmosphere acquired "*in situ"* and simultaneously with the moment of scene recording. The relative methods proceed under the assumption that the relationship between the at-sensor radiances recorded at two different times from regions of constant reflectance is spatially homogeneous and can be approximated by linear functions. The most difficult and time consuming aspect of all of these methods is the determination of suitable time-invariant features upon which to base the normalization.

In this paper the radiometric normalization techniques of Landsat ETM+ were analysed. These data were referred to acquisitions times comprised in 1999-2001-2002 years on a test area of southern Lazio. A normalization algorithm, based on MAD (*Multivariate Alteration Detection)* transformation, was implemented for this aim, by executing a quantitative and qualitative comparison with the consolidated ELC (*Empirical Line Calibration*) method.

1. INTRODUCTION

Management and environmental protection require a technology able to investigate, to measure and to monitor natural and atrophic dynamics. Conventional survey "*in situ*" techniques need high times and costs, unacceptable for public agencies sensitive to the safeguard and to the correct use of territory. Remote sensing offers an excellent opportunity to monitor regularly large surfaces, with comparatively reasonable times and costs.

In literature there are many techniques for multitemporal analysis and *Image differencing* is the most direct method. The simple difference among two co-registered satellite data, acquired in different times, offers a quantitative assessment of change percentage "point to point" (Nielsen et al., 1998).

The limits of this technique are connected to the difficulty to achieve absolute accuracy, to the temporal stability of sensor calibration, to the level of correlation of bands, to the atmospheric conditions and, finally, to the geometry of sun-earth-sensor. Such elements doesn't enable an effective comparison among images, because such data have not a common radiometric reference.

The radiometric normalization makes this technique particularly advantageous. In such cases is fundamental to correct radiometrically images, in order that information contained in a single *DN* (Digital Number) is lightly influenced by noise.

Absolute radiometric correction of multi-temporal satellite imagery requires atmospheric corrections associated with the atmospheric properties at the time of the image acquisition. Data for the characterisation of the relevant atmospheric processes modulating the incoming radiation at the satellite sensor require auxiliary data of parameters, such as the content of aerosols, ozone or water vapor in different atmospheric layers (Kaufmann, 1989; Mitchell and O'Brien, 1993). For historic satellite data such data are often difficult or impossible to obtain.

Whenever atmospheric parameters are not available and/or absolute surface radiances are not necessary, a relative normalisation of the satellite images to a master scene, based on the radiometric information intrinsic to the images, is an alternative ((Scott et al., 1988; Hall et al.,1991; Furby et al., 2001; Du et al., 2002). This is especially true in land cover classifications and post classification change detection applications (Song et al., 2001).

Radiometric normalisation, either relative or absolute, of imagery is important for many other applications, such as image mosaicing or tracking vegetation indices over time etc. (Yang and Lo, 2000). Furthermore, if change detection procedures, such as image differencing or change vector analysis, is preferred it must generally be preceded by radiometric normalisation (either absolute or relative).

All these techniques are not "corrections" in the sense that they use actual atmospheric measurements from the time of image acquisition, but rather attempt to uniformly minimize effects of changing atmospheric and solar conditions relative to a standard image selected by the user (Callahan, 2003).

Several methods as of Schott et al. (1988); Hall et al. (1991); Moran et al. (1995); Furby and Campbell (2001); Du et al. (2002) have been proposed for the relative radiometric normalisation of multispectral images taken under different conditions at different times. All proceed under the assumption that the relationship between the at-sensor radiances recorded at two different times from regions of constant surface reflection can be approximated by linear functions.

The most difficult and time-consuming aspect of all of these methods is the determination of suitable time invariant features upon which the normalisation is based. A further limit is the case in which satellite data are afflicted with intrinsic radiometric problems, as cloud or snow covers (Moran et al., 1992).

In this paper the radiometric normalization *scene-to-scene* with ELC (*Empirical Line Calibration*) and MAD (*Multivariate Alteration Detection)* techniques on Landsat ETM+ data had been analysed, by executing a quantitative and qualitative comparison. These data were referred to acquisitions times comprised in 1999-2001-2002 years on a test area of southern Lazio – Italy (Figure 1A-1B-1C). With the ELC technique Pseudo-Invariant Features (PIF) were manually selected, whereas the same Features were automatically identified with the aid of a normalization algorithm based on MAD transformation.

Figure 1A

Figure 1B

Figure 1C

2. METHODS OF ANALYSIS

The basic assumption of the most of scene-to-scene techniques is funded on a linear relation between resampled pixels of 'reference' or 'master' image and pixels of image to be normalized, denoted as 'target' or 'subject' (Casselles et al., 1989).

Schott et al. (1988) proposed that in the case of the availability of a large amount of homogeneously distributed invariant pixels, a regression of the same pixels would produce the best results, but assumed that these pixels are not identifiable. This would be satisfied if ground truth data of the true invariant pixel were available, which is rarely the case. Thus their idea was to introduce the term pseudo-invariant feature (PIF). PIFs are areas, assumed to be invariant but potentially exhibit some change pixels. PIFs need to be identified manually within bi- or multi-temporal images. Schott et al. (1988) proposed the usage of band ratios, Hall et al. (1991) a tasseled cap transformation to identify potential no-change pixels a priori.

The pseudo-invariant features are used for a stochastic estimation of regression coefficients for an image to image radiometric normalisation. The 'reference' denoted with DN_1, the image that is normalised to the master image is DN_2, and DN'_2 the normalised image; i represents the spectral bands. The following expression from Schott et al. (1988) was used for a radiometric normalisation:

$$\boldsymbol{DN'}_{2i} = \frac{\sigma_{1i}}{\sigma_{2i}} \boldsymbol{DN}_{2i} + \overline{\boldsymbol{DN}_{1i}} - \frac{\sigma_{1i}}{\sigma_{2i}} \overline{\boldsymbol{DN}_{2i}} \qquad [1]$$

where $\overline{\boldsymbol{DN}_{1i}}$ and $\overline{\boldsymbol{DN}_{2i}}$ are the means of the pseudo-invariant pixels of image 1 and 2 (next denoted in matrix form respectively as **F** and **G**); $\boldsymbol{\sigma_{1i}}$ and $\boldsymbol{\sigma_{2i}}$ are the respective standard deviations.

This formula can be reduced to a simplified expression of an independent variable x and a dependent variable y in the sense:

$$\boldsymbol{y = ax + c} \qquad [2]$$

with slope: $\boldsymbol{a} = \frac{\sigma_{1i}}{\sigma_{2i}}$

and intercept: $\boldsymbol{c} = \overline{\boldsymbol{DN}_{1i}} - \frac{\sigma_{1i}}{\sigma_{2i}} \overline{\boldsymbol{DN}_{2i}}$

Manual identification of invariant targets is subjective, laborious and with numerous errors. The regression procedure would need of targets selected on the whole range of values (*bright* - *midrange* - *dark*) with the same dimension and the same number. Every target would be localized in a flat area with regular characteristics, far from borders of the acquired scene, in order to minimize errors due to co-registration (Furby et.al., 2001).

In literature there are many techniques, f.i. PCA (Principal Components Analysis), to assist user in the selection of invariant features or *no-change* pixels (Du et al., 2002).

As in our study, this last is of limited effectiveness in presence of data with a high level of temporal and intrinsic change, and with invariant pixels in lower number in comparison with the remainder pixels of the whole image.

In image differencing techniques the invariant pixels are selected by means of the simple image difference (**F** and **G** matrixes or random vector) acquired in two different dates (t_1, t_2)

$$\mathbf{F} - \mathbf{G} = [\, F_1 - G_1 \ldots F_k - G_k \,]^T \qquad [3]$$

with

$\mathbf{F} = [\, F_1 \ldots F_k \,]^T$ and $\mathbf{G} = [\, G_1 \ldots G_k \,]^T$

k = band number.

Areas with a light rate of change will have a very low DN value. The limit of this procedure consists in lack of simultaneous comparison of all changes for all bands.

Although the principle is similar (invariant pixels are used in an regression approach), MAD transformation (Canty et al., 2004;

Canty, 2005) is new and fully automatic, overcoming the above-mentioned problems with the concentration of information on the global change rate. Moreover, it is invariant compared with linear effects caused by atmospheric conditions and sensor calibration (Nielsen et al., 1998). The main progress is the automatic identification of "no change pixels", that are homogeneously distributed over the entire image and different surface types.
In the first phase of the procedure a linear combination of all intensities of the N bands of the two images is supposed.

$$U = \mathrm{a}^{\mathrm{T}}\,\mathbf{F} = a_1 F_1 + a_2 F_2 + \ldots + a_N F_N \qquad [4]$$

$$V = \mathrm{b}^{\mathrm{T}}\,\mathbf{G} = b_1 G_1 + b_2 G_2 + \ldots + b_N G_N \qquad [5]$$

The a_i and b_i $(i = 1 \ldots N)$ vectors of coefficients are calculated in order to minimize the positive correlation between U and V. This means that the resulting difference image $U - V$ will show maximum spread in its pixel intensities.
If we assume that the spread is primarily due to actual changes that have taken place in the scene over the interval t_1- t_2,, then this procedure will enhance those changes as much as possible. Particularly we seek linear combinations such that

$$\mathrm{Var}(U\text{-}V) = \mathrm{Var}(U) + \mathrm{Var}(V) - 2\mathrm{Cov}(U,V) \rightarrow \max \qquad [6]$$

subject to the constrain

$$\mathrm{Var}(U) = \mathrm{Var}(V) = 1 \qquad [7]$$

we will have $\mathrm{Var}(U - V) = 2(1 - \rho)$ [8]

where $\rho = \mathrm{Corr}(U,V)$ is the correlation of the transformed vectors U and V.

Since we are dealing with change detection, we require that the random variables U and V be positively correlated, that is,

$\mathrm{Cov}(U,V) > 0$.

We thus seek vectors **a** nd **b** which minimize the positive correlation ρ.

The [6] procedure identifies N *sets* of coefficients a_i e b_i , where every set corresponds to a single difference component.

$$\mathrm{MAD}_i = U_i - V_i = a_i^{\mathrm{T}} F - b_i^{\mathrm{T}} G, \quad i = 1 \ldots N \qquad [9]$$

Consequently, the *no-change* pixels for radiometric normalization must satisfy the next relation

$$\sum_{i=1}^{N} \left(\frac{MAD_i}{\sigma_{MAD_i}} \right)^2 < t \qquad [10]$$

where $\sigma^2{}_{MAD_i} = 2(1 - \rho_i)$

and the decision threshold $t = \chi^2_{N,\,P=0.01}$

The term P is the probability to observe a lower value of t, in no change hypothesis, the [10] brings near to χ^2 with N degrees of freedom.

3. DATA AND RESULTS

The methods were evaluated and tested on three Landsat ETM+ data acquired over Aurunci chain, in southern Apennine of Lazio (Italy), on September 24, 1999, April 6, 2001 and February 2, 2002. The images were subset with dimensions 650 × 650 pixels (Figure 1A-1B-1C).
This territory was chosen because it presents a diversified morphology with active anthropical dynamics and permits to test the effectiveness of normalization alghoritm, both the consolidated (ELC) and the innovative (MAD) ones, even in not much favourable climatic and territorial situations. With this aim, satellite data acquired in different period of the year were analysed, with various atmospheric and illuminated conditions.

	A (February 2002) Target				**B** (April 2001) Target				**C** (September 1999) Reference			
Band	Min	Max	Mean	Stdev	Min	Max	Mean	Stdev	Min	Max	Mean	Stdev
1	43	162	59,68	5,27	64	255	90,98	23,76	58	236	77,21	7,49
2	24	141	43,89	6,69	42	255	73,04	24,06	38	251	59,10	8,80
3	17	171	42,34	10,29	33	255	68,17	28,51	29	255	55,96	14,12
4	13	139	53,75	17,38	16	244	73,77	23,40	18	255	85,63	21,94
5	6	220	51,46	21,48	15	255	78,39	29,68	12	255	73,77	23,54
7	4	255	34,48	14,67	11	255	50,76	23,54	8	255	46,11	17,00

Table 1 – Statistics of images

In Table 1 the DN ranger for single band are displayed. The maximum and minimum values for every band are very different among images. Such differences are due to the presence of clouds and snow covers in the whole acquisition scene (absent in test area of Figure 1A).
Before the execution of radiometric correction procedures, the images were co-registered, by identifying 30 GCP (*Ground Control Point*) by means of *Image-to-Image* technique of ENVI image processing software and using Landsat ETM+ data of 1999 as reference image. With this aim, a not parametric model, based on the 3° order polynomial function, was used and a value lower than 0.5 pixel for RMS was obtained. Next, Landsat ETM+ data of 2000 and 2002 were resampled with *Nearest Neighbour* method, in order to not alter heavily the radiometric content of images.
In the first phase of this study, related to ELC processing, the pixel indispensable to calculate the calibration parameters (*gain ed offset*) were manually selected from the ground truth data, by selecting 10 targets o invariant regions from the positional point of view and with similar radiometric characteristics. Table 2

shows the number of pixels distributed across different surface types to obtain the best regression estimation.
For every pixel in every band were executed the relationships given by these coefficients, to convert a digital count to a reflectance-resulting in the ELM calibrated image. ENVI refers to the slope curve as Solar Irradiance and the intercept curve as Path Radiance. The final output image is in reflectance space rather than radiance space.
In the second phase, MAD technique had permitted to automatically identify invariant pixels, while the calibration parameters were determined with orthogonal regression (Canty et al., 2004). The exactness of procedure was evaluated by means of the gains and the offset values (Table 3). Such values must be near respectively to one and zero (Du et al., 2002), in order to not loose the radiometric resolution in comparison to the initial data.
For both the procedures the gains and offsets values of band 6 were widely higher than values of remaining bands. This is due to the lower geometric resolution (60 m) and the intrinsic characteristics of bands that works in thermic range, and with electromagnetic radiation emitted rather than reflected.
A further validity control of procedures (Yuan et al., 1996) was carried out by means of MSE mean (*Mean Square Error*) on the 10 sample areas, each of 256 pixels, uniformly distributed on original image (Figure 3) and on normalized images.

	n° pixel	Band 1	Band 2	Band 3	Band 4	Band 5	Band 7	
Sand	25	105,88	92,24	102,92	85,76	93,72	76,44	SEPTEMBER 1999
Buildings	19	110,79	90,95	102,74	84,68	95,26	82,58	
Water	112	75,87	46,75	34,28	20,29	14,86	12,78	
Quarry	38	125,71	121,71	161,82	146,39	205,89	157,13	
Rock 1	65	90,42	75,49	78,52	112,92	120,15	75,28	
Rock 2	32	77,94	60,59	58,34	95,97	95,84	58,69	
Shaded slope	50	63,64	45,22	36,18	90,48	53,50	26,56	
Bare soil 1	30	74,73	58,67	66,97	59,43	68,17	51,90	
Bare soil 2	20	85,40	72,30	84,85	76,80	98,20	80,90	
Asphalted park	12	96,25	74,50	78,75	70,75	69,58	54,17	
Sand	25	114,28	99,40	110,60	69,12	101,24	79,36	APRIL 2001
Buildings	19	129,21	111,32	127,53	73,00	113,89	102,42	
Water	112	87,51	56,58	42,40	19,02	19,53	16,46	
Quarry	38	121,58	114,89	146,18	95,39	177,26	129,11	
Rock 1	65	103,66	87,20	89,37	81,78	125,88	84,89	
Rock 2	32	92,41	75,22	73,16	73,78	110,44	73,59	
Shaded slope	50	76,32	53,80	47,38	36,76	41,80	29,84	
Bare soil 1	30	79,07	62,13	64,40	57,97	65,63	42,83	
Bare soil 2	20	92,80	78,40	87,05	55,30	90,40	75,05	
Asphalted park	12	107,08	85,42	86,83	61,58	80,08	62,33	
Sand	25	75,16	61,04	66,20	56,28	63,32	52,32	FEBRUARY 2002
Buildings	19	83,05	67,84	78,89	64,11	72,53	66,79	
Water	112	58,20	36,61	27,33	15,44	9,59	8,73	
Quarry	38	86,82	84,92	117,18	110,92	171,47	126,87	
Rock 1	65	69,98	58,09	64,89	78,43	102,91	69,75	
Rock 2	32	60,59	45,84	48,72	57,31	75,59	52,13	
Shaded slope	50	49,36	31,22	26,72	26,18	24,14	17,20	
Bare soil 1	30	58,07	42,57	45,47	42,37	48,20	37,20	
Bare soil 2	20	66,90	54,30	62,75	52,95	68,60	57,90	
Asphalted park	12	70,33	53,25	54,50	48,75	46,25	37,42	

Table 2 – Mean of pseudo-invariant target used in ELC (*Empirical Line Calibration*) method

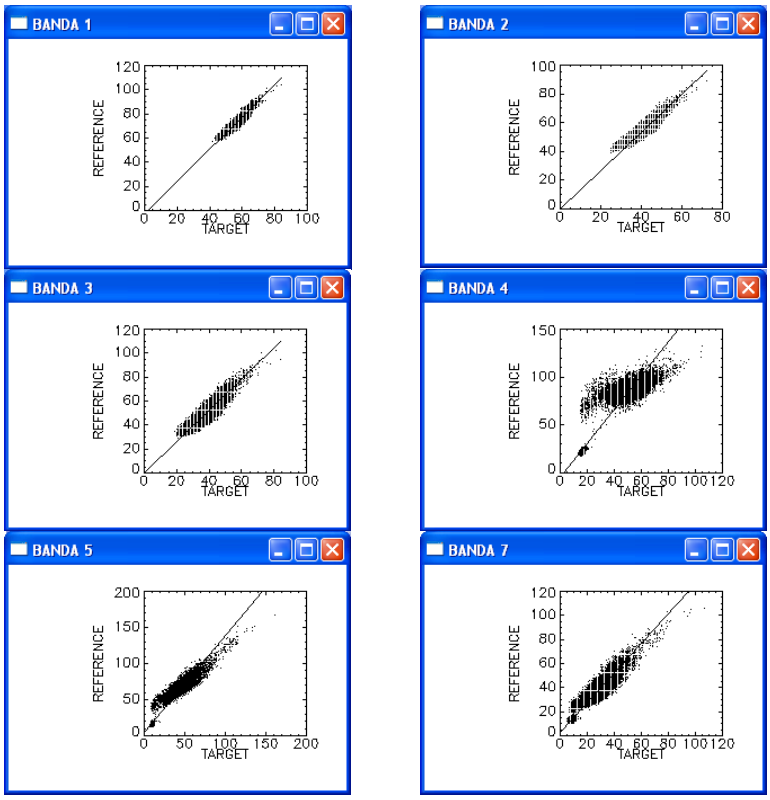

Figure 2. Sample scatter plots showing the results of equation of linear regression with ELC method

	ELC -Empirical Line Calibration				Radiometrical Calibration with MAD			
	A → C		B → C		A → C		B → C	
	Gain	Offset	Gain	Offset	Gain	Offset	Gain	Offset
Band 1	1,652	-21,412	1,137	-23,469	0,850	1,792	1,366	-4,472
Band 2	1,500	-6,535	1,137	-19,854	0,940	-7,013	1,307	1,445
Band 3	1,434	-4,463	1,163	-21,236	1,010	-8,842	1,345	-1,157
Band 4	1,412	6,280	1,769	-25,999	1,167	-0,459	1,587	1,841
Band 5	1,119	15,154	1,161	-16,013	1,030	-5,217	1,250	9,072
Band 7	1,209	3,989	1,236	-18,390	1,039	-4,437	1,210	4,028

Table 3: Results of gains and offsets obtained with ELC and MAD methods.

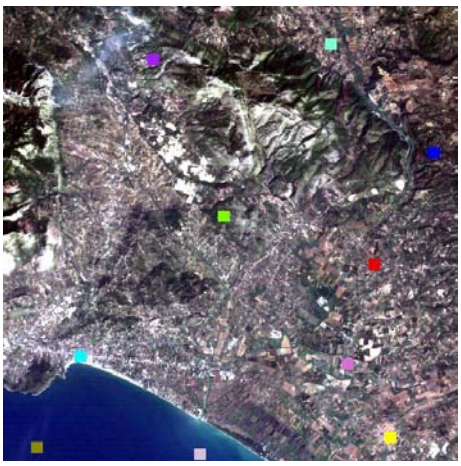

Figure 3: Test areas location

MSE mean	A normalized on C			B normalized on C		
1	149,61	27,20	13,71	137,49	86,36	6,03
2	170,74	29,98	15,90	145,06	78,83	5,10
3	675,58	66,77	71,38	346,14	187,14	125,87
4	479,11	84,72	88,20	327,21	105,42	120,50
5	604,58	124,99	131,07	297,82	81,02	78,93
6	668,07	128,75	127,17	402,06	187,39	181,26
7	471,30	101,93	108,53	294,60	160,23	104,73
8	499,92	65,79	56,66	178,58	372,40	177,69
9	679,71	127,06	119,22	447,19	166,21	193,40
10	524,34	98,70	82,07	249,63	86,90	35,93

Table 4: Values of MSE for every test areas

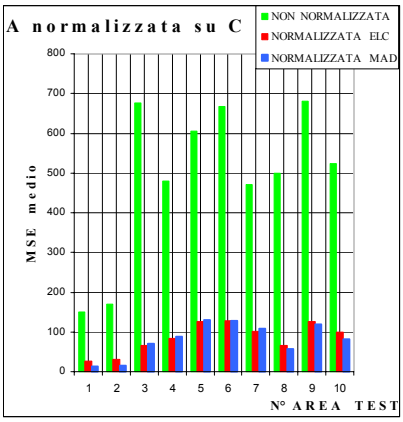

Figure 3a: Histogram of MSE values related to normalization of image A on C

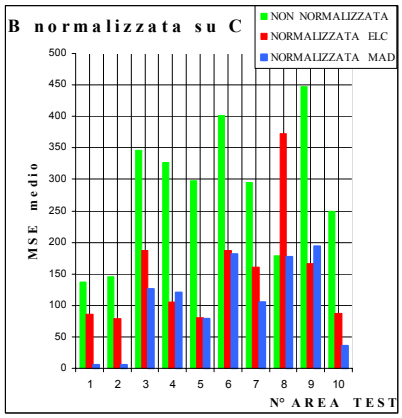

Figure 3b: Histogram of MSE values related to normalization of image B on C

4. CONCLUSION

The analysis of the results (Table 4, Figure 3a and Figure 3b) demonstrated the validity of the innovative technique MAD for radiometric normalization of multitemporal satellite data. On the whole, the MAD based normalisation and the ELC based normalisation technique generally produce comparable results for images with light level of noise (Figure 1A compared with Figure 1C).

A certain amount of problems were proved on image with intrinsic radiometric problems, such as haze phenomenon and cloud covers (Figure 1B, Figure 3b). Some relevant discrepancies were found on the class bare soil 2, probably because of clear differentiation with the class bare soil 1.

Generally, the mean values after the image normalisation in both approaches are well represented. The variances of the no change pixels in both normalisation approaches are slightly underestimated. The regression parameters on the no change pixels are slightly better represented in the MAD based approach.

Due to its completely automatic operation, and as parameters are free and fast, the MAD based normalisation technique was favoured, as the definition of decision thresholds or individuation of PIF (*Pseudo Invariant Features*) with subjective criterions by using ELC techniques.

In fact, with MAD transformation the basic data come completely from the same image, without interference of unfavourable climatic conditions or every type of noise/variation in terms of reflectance (Canty et al., 2004).

ACKNOWLEDGMENTS

The authors appreciate the support of Prof. A. Leone and Dr. F. Recanatesi - University of La Tuscia (Viterbo) - for making available satellite images used for this study.

REFERENCES

Callahan, K., E., (2003), Validation of a radiometric normalization procedure for satellite derived imagery within a change detection framework, thesis of MS in Geography, Logan, Utah.

Canty M. J., Nielsen A. A., Schmidt M. (2004), Automatic radiometric normalization of multitemporal satellite imagery. Remote Sensing of Environment, 91, 4411-451.

Canty M. J., CDSAT.ZIP - ENVI plug-ins for change detection in multispectral satellite imagery, http://www.fz-juelich.de/ste/remote_sensing, May 2005.

Casselles V., Garcia M. Y. L. (1989), An alternative simple approach to estimate atmospheric correction in multitemporal studies. International Journal of remote sensing, 10, 1127-1134.

Du Y., Teillet P.M., Cihlar J. (2002), Radiometric normalization of multitemporal high-resolution images with quality control for land cover change detection. Remote sensing of Environment, 82, 123-134.

Furby S. L., Campbell N. A. (2001), Calibrating images from different dates to 'like-value' digital counts. Remote sensing of Environment, 77, 186-196.

Hall F. G., Strebel D. E., Nickeson J. E., Goetz S. J. (1991), Radiometric rectification: Toward a common radiometric response among multidate, multisensor images. Remote sensing of Environment, 35, 11-27.

Moran M. S., Jackson R. D., Slater P. N., Teillet P. M. (1992), Evalution of simplified procedures for retrival of land surface reflectance factors from satellite sensor output. Remote sensing of Environment, 41, 160-184.

Nielsen A. A., Conradsen K., Simpson J. J. (1998), Multivariate alteration detection (MAD) and MAF post-processing in multispectral bitemporal image data: New approaches to change detection studies. Remote Sensing of Environment, 64, 1-19.

Schott J.R., Salvaggio C., Volchok W.J. (1988), Radiometric scene normalization using pseudo- invariant features. Remote Sensing of Environment, 26, 1-16.

Yuan, D., Elvidge, C. D. (1996), Comparison of relative radiometric normalization techniques, Photogrammetry & Remote Sensing, 51, 117-12